Survey of upper band chorus and ECH waves: Implications for the diffuse aurora

Nigel P. Meredith,[1] Richard B. Horne,[1] Richard M. Thorne,[2] and Roger R. Anderson[3]

Received 10 March 2009; revised 1 May 2009; accepted 11 May 2009; published 18 July 2009.

[1] The origin of the diffuse aurora has been a source of controversy for many years. More recently, the question has taken a new significance in view of the associated changes in atmospheric chemistry which may affect the middle atmosphere. Here, we use CRRES data to assess the importance of upper band chorus and electron cyclotron harmonic (ECH) waves in the production of the diffuse aurora. Both wave modes increase with increasing geomagnetic activity, suggesting they are related to periods of enhanced convection and/or substorm activity. They are confined to the near-equatorial region, which excludes the prenoon sector from the wave survey. During active conditions, intense ECH waves and upper band chorus, with amplitudes exceeding 1 mV m^{-1}, are observed in the region $4 < L < 7$ from 2100 to 0600 MLT approximately 20% and 6% of the time, respectively. This suggests that both wave modes can put electrons on strong diffusion, but only during active conditions and not at all local times. Scattering rates fall below the strong diffusion limit at other times when the wave amplitudes are weaker. Fluxes of low energy electrons (100 eV < E < 30 keV) also increase with increasing geomagnetic activity in approximately the same region of geospace as the waves, suggesting that these electrons are responsible for the generation of the waves. The patterns of the upper band chorus, ECH waves, and low-energy electrons are similar to the global morphology of the diffuse aurora, suggesting that both wave modes play significant roles in the production of the diffuse aurora.

Citation: Meredith, N. P., R. B. Horne, R. M. Thorne, and R. R. Anderson (2009), Survey of upper band chorus and ECH waves: Implications for the diffuse aurora, *J. Geophys. Res.*, *114*, A07218, doi:10.1029/2009JA014230.

1. Introduction

[2] The diffuse aurora is a weak belt of emissions extending around the entire auroral oval which comprises 80% of the total auroral energy input into the polar region at solar maximum and 50% at solar minimum [*Sandford*, 1968]. The region extends over a latitude range of 5°–10° and, following geomagnetic field lines, maps out to the entire central plasma sheet. The diffuse aurora is thus a major energy source in the high latitude ionosphere. Indeed, changes in the ionospheric structure at high latitudes, driven by the diffuse aurora, can have significant effects on communications and radar systems. Furthermore, the effects of the diffuse aurora, including both the direct electron and bremsstrahlung contributions, on mesospheric and stratospheric chemistry may be significant [*Frahm et al.*, 1997].

[3] The diffuse aurora is the result of pitch angle scattering of plasma sheet electrons in the energy range from 100 eV to several keV into the loss cone by wave-particle interactions [*Fontaine and Blanc*, 1983] and forms an important loss mechanism for plasma sheet particles. Both electron cyclotron harmonic (ECH) waves and whistler mode chorus resonate with electrons in this energy range and have been associated with enhanced fluxes of low energy electrons [*Anderson and Maeda*, 1977]. However, which of these two mechanisms is more influential in the production of the diffuse aurora remains a subject of controversy in magnetospheric physics. [e.g., *Belmont et al.*, 1983, 1984; *Lyons*, 1984; *Roeder and Koons*, 1989; *Johnstone et al.*, 1993; *Meredith et al.*, 1999, 2000; *Horne and Thorne*, 2000; *Horne et al.*, 2003; *Ni et al.*, 2008].

[4] ECH waves are electrostatic emissions observed in bands between the harmonics of the electron gyrofrequency, f_{ce}, and sometimes referred to as $(n + 1/2)f_{ce}$ waves since they tend to be observed in narrow bands close to odd integral half-harmonics of the electron gyrofrequency [e.g., *Kennel et al.*, 1970; *Fredericks and Scarf*, 1973; *Shaw and Gurnett*, 1975; *Christiansen et al.*, 1978; *Gurnett et al.*, 1979]. They were first reported by *Kennel et al.* [1970] from OGO-5 data. Both theoretical and detailed data modeling show that they are generated by a loss cone distribution [*Ashour-Abdalla and Kennel*, 1978; *Rönnmark and Christiansen*, 1981; *Horne et al.*, 1981]. Various classification schemes have since been introduced to characterize these various spectral types [e.g., *Hubbard and Birmingham*, 1978;

[1]British Antarctic Survey, Natural Environment Research Council, Cambridge, UK.
[2]Department of Atmospheric and Oceanic Sciences, University of California, Los Angeles, California, USA.
[3]Department of Physics and Astronomy, University of Iowa, Iowa City, Iowa, USA.

0148-0227/09/2009JA014230

Gough et al., 1979]. The emissions are localized to within a few degrees of the magnetic equator [*Gough et al.*, 1979; *Christiansen et al.*, 1978; *Paranicas et al.*, 1992] and are seen most frequently in the region from 2100 to 0600 MLT for $4 < L < 8$ [*Roeder and Koons*, 1989].

[5] Typical amplitudes reported from OGO-5 observations were very large, ranging from 1 to 10 mV m^{-1} and sometimes as high as 100 mV m^{-1} [*Kennel et al.*, 1970]. These amplitudes are large enough to cause strong pitch angle diffusion for electrons with energies from a few hundred eV to several keV, suggesting that these waves could be responsible for the diffuse aurora [*Lyons*, 1974]. However, a decade or so later, *Belmont et al.* [1983] reported more modest levels of ECH wave activity using data from the geostationary GEOS 2 satellite. They showed that, within 3° of the magnetic equator in the region 2200–0600 MLT, a wave amplitude of 1 mV m^{-1} was exceeded during only 2% of the time and that most (88%) of the time the signal was much weaker and less than 0.1 mV m^{-1}. Since the minimum wave amplitude for strong diffusion is expected to exceed 2 mV m^{-1} for a resonant particle of energy 1 keV, *Belmont et al.* [1983] concluded that the occurrence and intensity of ECH waves were too small to account for the continuous precipitation of electrons in the diffuse aurora.

[6] Another type of wave that can cause precipitation of plasma sheet electrons is whistler mode chorus. These waves, which are electromagnetic in nature, are observed outside the plasmapause in the frequency range from 0.1 to $0.8f_{ce}$ [*Tsurutani and Smith*, 1977; *Koons and Roeder*, 1990]. The emissions are often observed in two distinct bands, referred to as upper ($0.5f_{ce} < f < f_{ce}$) and lower ($0.1f_{ce} < f < 0.5f_{ce}$) band chorus, with a gap at $0.5f_{ce}$ [*Tsurutani and Smith*, 1974]. Electrons with energies of the order of a keV or so tend to resonate with upper band chorus [*Inan et al.*, 1992; *Johnstone et al.*, 1993]. This emission is substorm dependent and maximizes during active conditions near the magnetic equatorial plane on the nightside [*Meredith et al.*, 2001]. During such conditions, the rate of pitch angle scattering by upper band chorus can exceed the level of strong diffusion over a broad energy range below a few keV [*Ni et al.*, 2008]. At higher energies, lower band chorus provides more effective scattering, especially near the loss cone [*Ni et al.*, 2008]. Chorus scattering could thus also play a major role in the production of the diffuse aurora, particularly during active times.

[7] *Meredith et al.* [1999, 2000] studied the evolution of highly anisotropic electron distributions, peaked at 90° pitch angle, in the energy range 100 eV < E < 30 keV. These distributions, known as pancake distributions [*Wrenn et al.*, 1979], were seen to evolve from freshly injected isotropic distributions on a timescale of the order of 4 hours. The particle injections were accompanied by large amplitude (1 mV m^{-1}) ECH and whistler mode waves. Both wave modes decayed in amplitude on a timescale similar to that for pancake formation, suggesting that pancake distributions are a result of pitch angle scattering due to both wave types. Moreover, the timescale for pancake production and wave decay were found to be comparable with the average time interval between substorms, suggesting that these wave-particle interactions are almost continuous leading to a continual supply of electrons to power the diffuse aurora. *Horne et al.* [2003] subsequently examined a weak substorm event associated with enhanced whistler mode hiss, whistler mode chorus and ECH waves. Analysis of the resonant energies during propagation showed that while the ECH waves could resonate with the electrons from a few hundred eV to a few keV, the observed chorus and hiss were only able to resonate with electrons below and above this range respectively, suggesting that the ECH waves were responsible for the production of the diffuse aurora in this particular case.

[8] Early studies assumed that strong diffusion is required for the production of the diffuse aurora. However, *Chen and Schulz* [2001a] found that strong diffusion scattering overestimates the auroral precipitation at midnight while underestimating the precipitation near dawn. In a follow-on study *Chen and Schulz* [2001b] found that more realistic simulations of the diffuse aurora are produced by models in which the scattering rates are below the strong diffusion level, with an MLT dependence based on statistical wave data.

[9] *Peticolas et al.* [2002] conducted a case study of a black aurora using conjugate optical sensors and measurements from the FAST satellite. In the surrounding diffuse aurora the electron fluxes were isotropic at all energies. In contrast, in the black aurora, the loss cone fluxes were depleted for E > 2 keV. The authors concluded that ECH waves and chorus were responsible for the precipitation in the diffuse aurora whereas the black aurora was caused by the suppression of chorus. *Sergienko et al.* [2008] investigated the fine structure of the diffuse aurora using sensitive ground-based imagers and FAST electron measurements. They concluded that strong pitch angle diffusion driven by ECH waves was responsible for the background diffuse aurora, while the fine structure, which appeared as auroral stripes in the images, was created by the precipitation of electrons with energies above 3–4 keV as a result of pitch angle diffusion by whistler mode waves.

[10] Surveys of ECH waves have largely concentrated on the occurrence of emissions [e.g., *Fredricks and Scarf*, 1973; *Belmont et al.*, 1983; *Roeder and Koons*, 1989; *Koons and Roeder*, 1990], and, while a statistical survey of the average amplitudes of upper band chorus observed within ±15° of the magnetic equator has been presented [*Meredith et al.*, 2001], the global morphology and frequency structure of both wave modes close to the magnetic equator, where the waves are most intense, have not been studied in detail. Since accurate quantification of electron losses due to upper band chorus and ECH waves are essential for the refinement of models of the diffuse aurora, here we conduct a statistical survey of the amplitudes of upper band chorus and ECH waves using CRRES data to determine the global distribution of the waves as a function of geomagnetic activity to help determine where the waves should be most effective in driving the diffuse aurora. We also investigate one source of free energy that could drive the waves unstable by conducting a statistical survey of the flux of low energy electrons using CRRES particle data.

2. Instrumentation

[11] The Combined Release and Radiation Effects Satellite, CRRES [*Johnson and Kierein*, 1992], is particularly

well suited to studies of wave-particle interactions in the inner magnetosphere both because of its orbit and sophisticated suite of wave and particle instruments. This satellite, which was launched on 25 July 1990, operated in a highly elliptical geosynchronous transfer orbit with a perigee of 305 km, an apogee of 35,768 km and an inclination of 18°. The orbital period was approximately 10 hours, and the initial apogee was at a magnetic local time (MLT) of 0800 MLT. The magnetic local time of apogee decreased at a rate of approximately 1.3 hours per month until the satellite failed on 11 October 1991, when its apogee was at about 1400 MLT. The satellite covered a range of L from $L = 1.05$ to $L = \sim 8$ and a range of magnetic latitudes within ±30° of the magnetic equator, sweeping through the inner magnetosphere approximately 5 times per day, providing good coverage of this important region for almost 15 months.

[12] The wave data used in this study were provided by the Plasma Wave Experiment on board the CRRES spacecraft. This experiment provided measurements of the wave electric fields using a 100 m tip-to-tip long wire antenna, with a dynamic range covering a factor of at least 10^5 in amplitude [*Anderson et al.*, 1992]. The sweep frequency receiver, used in this study, covered the frequency range from 100 Hz to 400 kHz in four bands with 32 logarithmically spaced steps per band, the fractional step separation, $\Delta f/f$ being about 6.7% across the entire frequency range. Band 1 (100 to 810 Hz) was sampled at one step per second with a complete cycle time of 32.768 s. Band 2 (810 Hz to 6.4 kHz) was sampled at two steps per second with a complete cycle time of 16.384 s. Band 3 (6.4 to 51.7 kHz) and band 4 (51.7 to 400 kHz) were each sampled 4 times per second, with complete cycling times of 8.192 s. The nominal bandwidths in bands 1, 2, 3, and 4 were 7 Hz, 56 Hz, 448 Hz, and 3.6 kHz, respectively. The electric field detector was thus able to detect waves from below the lower hybrid resonance frequency(f_{LHR}) to well above the upper hybrid resonance frequency (f_{UHR}) for a large fraction of each orbit.

[13] The particle data used in this study were collected by the Low Energy Plasma Analyzer (LEPA). This instrument consisted of two electrostatic analyzers with microchannel plate detectors, each with a field of view of 120° × 5°, one measuring electrons and the other positive ions in the energy range 100 eV < E < 30 keV [*Hardy et al.*, 1993]. The instrument detected the complete pitch angle range from 0° to 180° every 30 s with a resolution of 5.625° × 8° at 20 energy channels in the range 100 eV < E < 30 keV.

3. CRRES Database

[14] In order to perform a statistical analysis of the occurrence of upper band chorus and ECH waves, together with one source of free energy that can drive the waves unstable, we constructed a database of the wave amplitudes and electron flux using the CRRES data. The wave data were initially corrected for the instrumental background response and smoothed by using a running 3 minute average to take out the beating effects due to differences in the sampling and the spin rate. Spurious data points, data spikes, and periods of instrumental downtime were flagged and ignored in the subsequent statistical analyses. Twelve orbits, during which nontraditional configurations were deployed for testing purposes, were also excluded from the analyses. The wave amplitude for a given band was obtained by integrating the measured wave spectral intensity in $V^2m^{-2}Hz^{-1}$ over the appropriate frequency band to obtain the intensity in V^2m^{-2} and then subsequently taking the square root to obtain the amplitude in Vm^{-1}.

[15] The electric field wave amplitudes for upper band chorus ($0.5f_{ce} < f < f_{ce}$) together with the ECH waves in the first harmonic band ($f_{ce} < f < 2f_{ce}$) were rebinned as a function of half orbit (outbound and inbound) and L in steps of 0.1 L. For more detailed spectral analysis the electric field wave amplitudes from $0.5f_{ce}$–$2f_{ce}$ and $2f_{ce}$–$5f_{ce}$were rebinned at the same spatial resolution in steps of $0.1f_{ce}$ and $0.2f_{ce}$ respectively. The electron differential number flux at 90° pitch angle for each energy level of the LEPA instrument, was also rebinned as a function of half orbit (outbound and inbound) and L in steps of 0.1 L. The data were recorded together with the universal time (UT), magnetic latitude (λ_m), magnetic local time (MLT), and time spent in each bin with the same resolution. The L value and magnetic latitude were determined using the Olson-Pfitzer tilt-dependent static model [*Olson and Pfitzer*, 1977] and the IGRF 85 model. The resulting database, consisting of wave and particle measurements from 939 orbits, was subsequently analyzed to determine the global morphology of the wave amplitudes and the electron fluxes as a function of geomagnetic activity.

4. CRRES Wave Observations

[16] An example of enhanced chorus and ECH wave activity which occurred during a period of enhanced geomagnetic activity on the 16/17 January 1991 is shown in Figure 1. Here the wave electric field spectral intensity is plotted against UT for an entire orbit of the CRRES spacecraft beginning at perigee at 1822:11 on 16 January 1991 and ending at the next perigee at 0415:50 on 17 January 1991. The magnetic local time, magnetic latitude, and L value are also given at hourly intervals. The solid white line shows the value of f_{ce}, determined from the measured ambient magnetic field, and the dashed white lines below f_{ce} represent $0.5f_{ce}$, $0.1f_{ce}$ and the lower hybrid resonance frequency, f_{LHR} respectively. The dotted white lines above f_{ce} correspond to the first four harmonics of f_{ce}. The dashed red line is the upper hybrid resonance frequency, f_{UHR}, calculated from wave emissions at f_{UHR} inside the plasmapause, and the solid red line denotes $f_{UHR} = (f_{pe}^2 + f_{ce}^2)^{1/2}$ calculated from the lower frequency cutoff of the electromagnetic continuum, which is taken to be a plasma wave cutoff at f_{pe} [*Gurnett and Shaw*, 1973]. The variation of the *AE* index during the orbit is shown in the top panel and is indicative of predominantly moderate activity (100 < *AE* < 300 nT) between 2100 UT on 16 January and 0300 UT on 17 January.

[17] Weak plasmaspheric hiss is observed below 2 kHz inside the plasmapause on both the outbound and inbound legs. This emission is largely responsible for the formation of the slot region [e.g., *Lyons and Thorne*, 1973; *Meredith et al.*, 2007, 2009], and the quiet time decay of radiation belt electrons in the inner region of the outer radiation belt [*Meredith et al.*, 2006; *Summers et al.*, 2007; *Lam et al.*, 2007]. On exiting the plasmapause at 2110 UT weak ECH

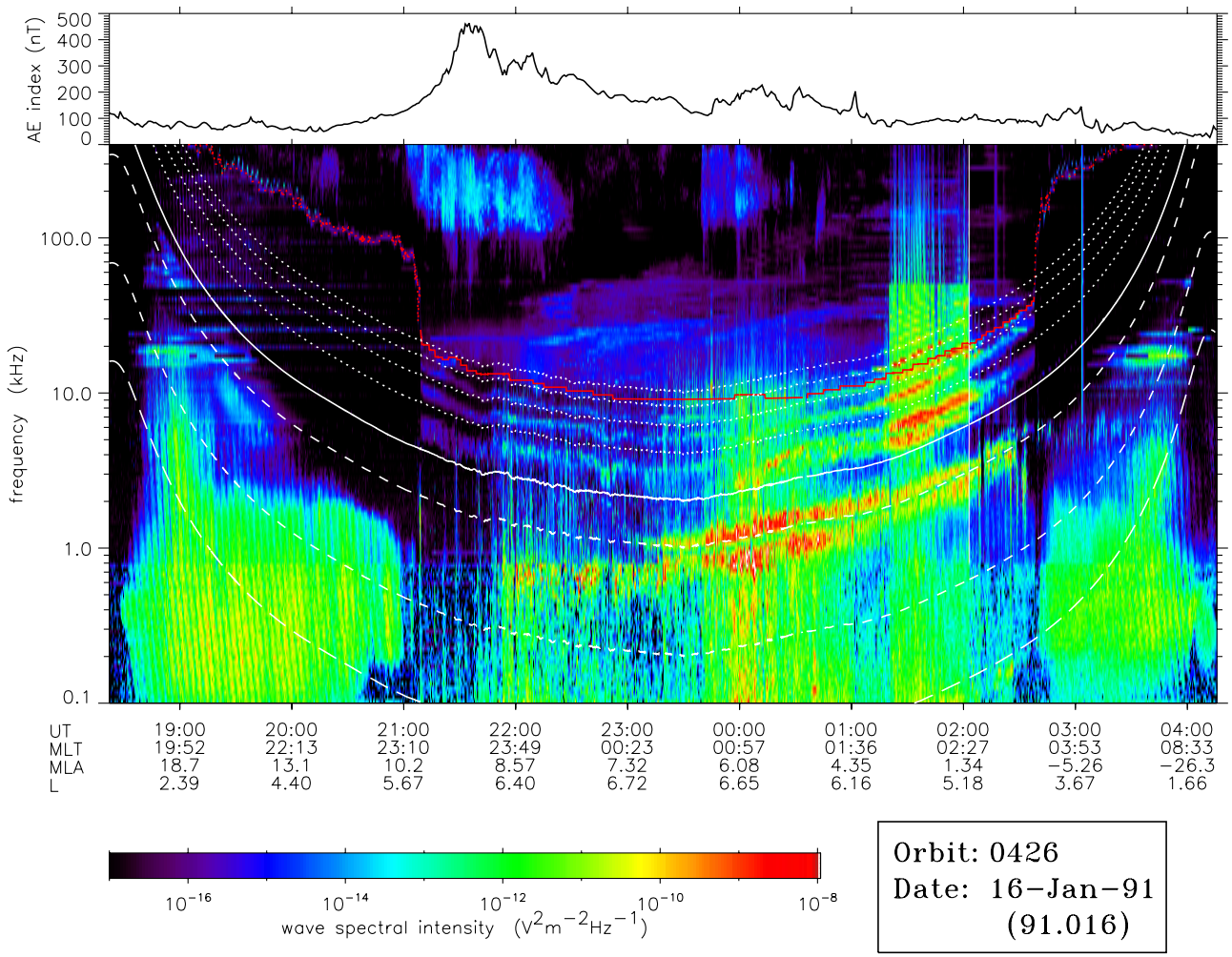

Figure 1. Survey plot of the wave spectral intensity observed on CRRES during orbit 426 together with a trace of the *AE* index. The solid white line shows the value of f_{ce}, and the dashed white lines below f_{ce} represent $0.5f_{ce}$, $0.1f_{ce}$, and the lower hybrid resonance frequency f_{LHR}. The dotted white lines above f_{ce} correspond to the first four harmonics of f_{ce}. The solid red line denotes the upper hybrid resonance frequency f_{UHR} calculated from the lower frequency cutoff of the electromagnetic continuum and the red dashed line is f_{UHR} calculated from wave emissions at f_{UHR} inside the plasmapause.

waves are seen in the first three harmonic bands. As the spacecraft approaches the magnetic equator the ECH waves become more enhanced. The strongest waves are seen between 0115 and 0205 UT, as the spacecraft moves from a magnetic latitude of 3.8° to 1.0°. In this region the waves have considerable structure. In the first harmonic band the emissions are double-banded with peak emissions near $1.1f_{ce}$ and $1.5f_{ce}$. In the second harmonic band the wave emissions peak in the center of the band, whereas in the third and fourth harmonic bands the emissions maximize low in the band. The waves become substantially weaker after 0205 UT and remain weak until disappearing completely at the inbound plasmapause crossing at 0238 UT. Sporadic chorus emissions first appear outside the plasmapause in the lower band around 2155 UT. They become accompanied by upper band chorus around 2330 UT after which chorus is observed in both bands right up until the inbound plasmapause crossing. The most intense chorus emissions are seen between 2345 and 0100 UT, somewhat earlier and at a higher magnetic latitude than the most intense ECH waves. The horizontal lines between 10 and 25 kHz before 2000 UT and after 0300 UT are from ground-based VLF transmitters used for navigation and communication with submarines.

5. Global Morphology of Upper Band Chorus and ECH Waves

5.1. Latitudinal Distribution

[18] The average wave amplitudes of the ECH waves in the first harmonic band ($f_{ce} < f < 2f_{ce}$) for the evening to dawn sector (2100–0600 MLT), where the waves are most prevalent [e.g., *Roeder and Koons*, 1989], are shown as a function of the radial distance from the center of the Earth projected onto the plane of the magnetic equator, x, SM z, and geomagnetic activity in the upper panels of Figure 2. The results are presented for three geomagnetic activity levels which, from left to right, are defined as quiet ($AE^* <$ 100 nT), moderate ($100 < AE^* < 300$ nT) and active ($AE^* >$ 300 nT). Here AE^* is the maximum value of the *AE* index in

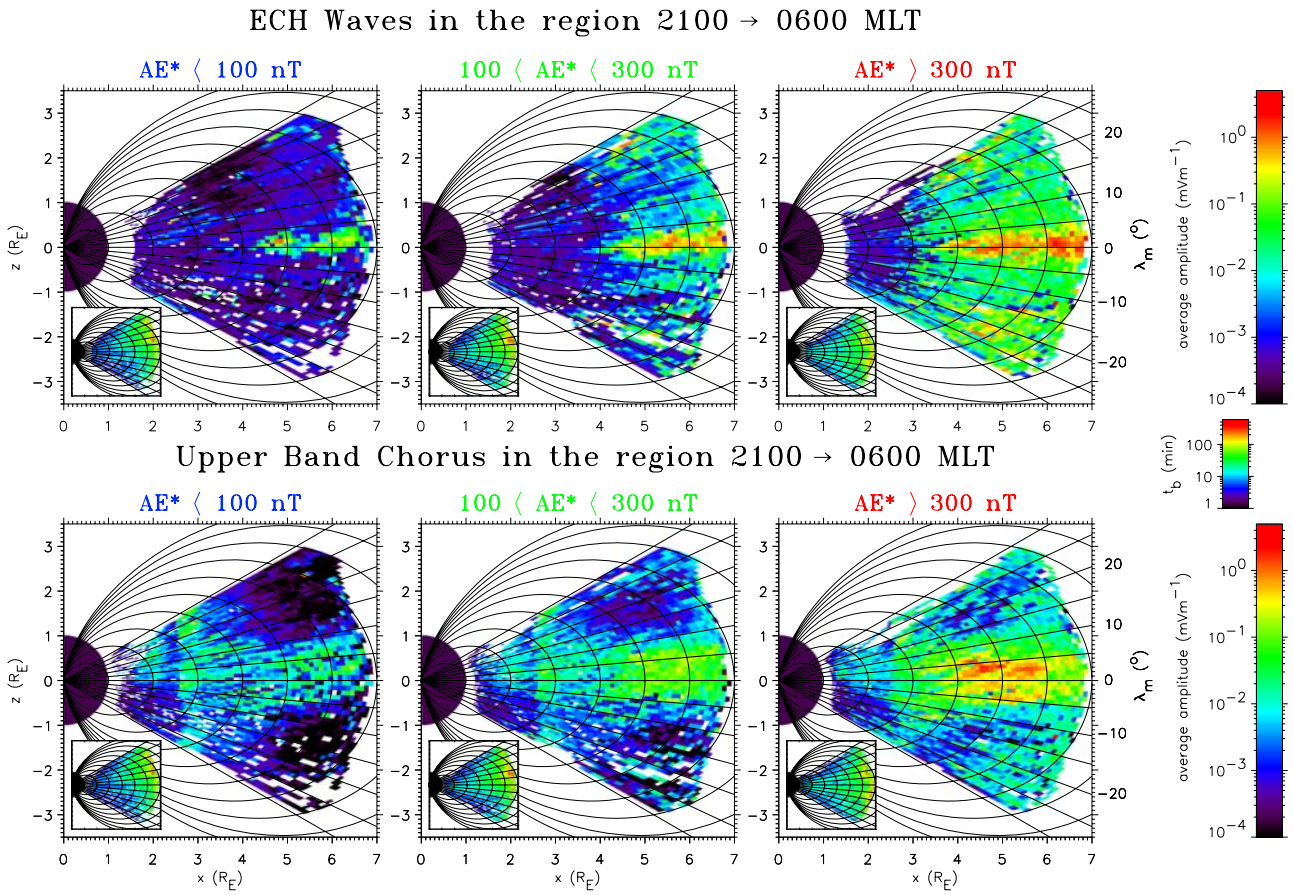

Figure 2. Average wave electric field amplitudes of (top) ECH waves and (bottom) upper band chorus in the sector 2100–0600 MLT as a function of the radial distance from the center of the Earth projected onto the plane of the magnetic equator, x, and SM z. From left to right, the results are presented for quiet ($AE^* < 100$ nT), moderate ($100 < AE^* < 300$ nT), and active ($AE^* > 300$ nT) conditions. The average amplitudes are shown in the large panels, and the corresponding sampling distributions are in the small panels.

the previous 3 hours, used to roughly take into account the drift time of the low energy electrons from the nightside neutral line to the inner magnetosphere [e.g., *Chen and Schulz*, 2001a]. Dipole field lines and lines of constant magnetic latitude are included to help visualize the behavior of the wave amplitudes as a function of L and magnetic latitude. The average amplitudes are plotted in the large panels and the corresponding sampling distributions are plotted in the smaller panels. Weak ECH emissions, typically less than 0.1 mV m^{-1}, are seen during quiet conditions (top left) but only in the region $L > 4.5$ and within a few degrees of the magnetic equator. These emissions become more enhanced during moderate conditions and extend to slightly lower L, where they remain confined to the equatorial region with peak amplitudes in the range $0.4 < E < 0.8$ mV m^{-1}. The most enhanced emissions are seen during active conditions (top right) in the region $3.5 < L < 7.0$ within ±3° of the magnetic equator, where the wave amplitudes can exceed 1 mV m^{-1}, particularly in the region outside $L = 6.0$.

[19] The upper band chorus amplitudes are shown in a similar format in the bottom panels of Figure 2. Weak upper band chorus emissions, ~0.01 mV m^{-1}, are seen during quiet conditions (bottom left) within 10° of the magnetic equator in the region $L > 4.5$. These emissions intensify during moderate conditions and extend to slightly lower L. The waves are most intense during active conditions (bottom right) in the region $L > 4$ within ±5° of the magnetic equator. Here the wave amplitudes can also exceed 1 mV m^{-1}, particularly in the region $4 < L < 6$. Weak emissions are also seen closer to the planet, $L < \sim 4.5$, primarily during quiet and moderate conditions which appear to be independent of geomagnetic activity. These emissions, which lie inside the plasmapause, have been attributed to signals from lightning and ground-based transmitters as discussed by *Meredith et al.* [2001].

5.2. MLT Distribution

[20] The average equatorial ($-3° < \lambda_m < 3°$) wave amplitudes of the ECH waves in the first harmonic band are shown as a function of L and MLT in the top panels of Figure 3. The plots extend linearly out to $L = 8$ with noon at the top and dawn to the right. From left to right the results are presented for quiet ($AE^* < 100$ nT), moderate ($100 < AE^* < 300$ nT), and active ($AE^* > 300$ nT) conditions. There is restricted coverage of the near-equatorial region

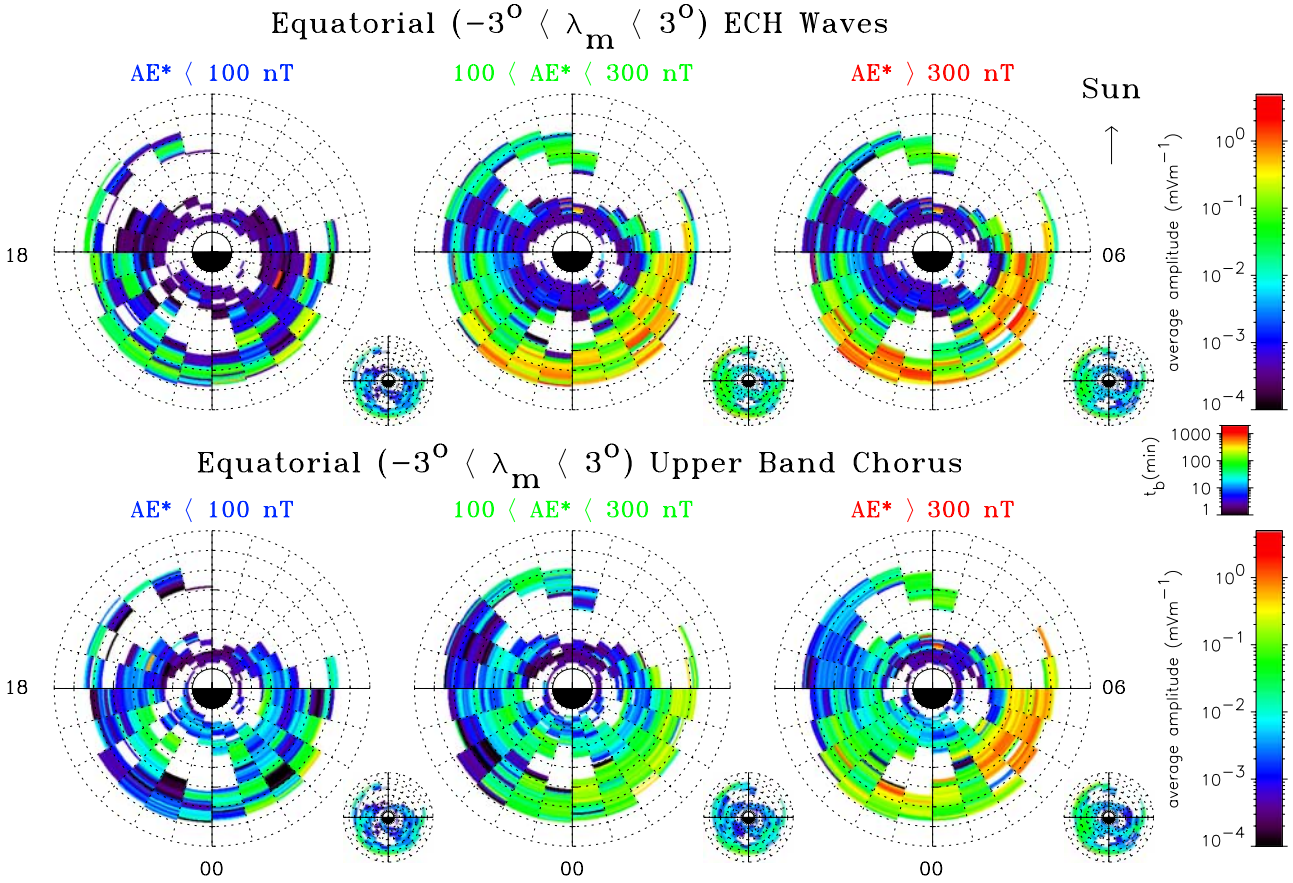

Figure 3. Average equatorial ($-3 < \lambda_m < 3°$) wave electric field amplitudes of (top) ECH waves and (bottom) upper band chorus as a function of L and magnetic local time. From left to right, the results are presented for quiet ($AE^* < 100$ nT), moderate ($100 < AE^* < 300$ nT), and active ($AE^* > 300$ nT) conditions. The average amplitudes are shown in the large panels, and the corresponding sampling distributions are in the small panels.

during the CRRES mission particularly in the prenoon sector. Weak emissions are generally seen during quiet conditions (top left) on the nightside with amplitudes typically less than 0.1 mV m^{-1} in the region $4.5 < L < 7.0$. The emissions intensify during moderate conditions particularly in the region 2100–0600 MLT. The most enhanced emissions are seen during active conditions (top right) and tend to be at larger L in the premidnight sector and lower L in the predawn sector.

[21] The upper band chorus emissions are shown in a similar format in the bottom panels of Figure 3. Weak emissions, with amplitudes generally less than 0.05 mV m^{-1} are seen on the nightside during quiet conditions (bottom left). The emissions intensify during moderate conditions with amplitudes in the range $0.05 < E < 0.2$ mV m^{-1} being observed in the region $L > 4$ from 2100 to 0600 MLT. The emissions are most intense during active conditions (bottom right) where the amplitudes can exceed 1 mV m^{-1} predominantly in the region $4 < L < 6$ between 0200 and 0600 MLT.

[22] The occurrence rates for equatorial ($-3 < \lambda_m < 3°$) wave amplitudes exceeding a given threshold for (top) ECH waves and (bottom) upper band chorus are shown as a function of L and magnetic local time in Figure 4. The results are shown for active conditions and, from left to right, for threshold amplitudes of 0.01, 0.1 and 1.0 mV m^{-1}. For ECH waves in the region $4 < L < 7$ from 2100 to 0600 MLT, wave amplitudes of 0.01, 0.1 and 1 mV m^{-1} are exceeded for 79%, 51%, and 20% of the time respectively. In the same region, the upper band chorus amplitudes exceed the same thresholds 73%, 47%, and 6% of the time respectively. The most intense waves tend to be seen in the region $4 < L < 6$ from 0200–0600 MLT. In this region the wave amplitudes exceed 1 mV m^{-1} for 27% and 18% of the time for ECH waves and upper band chorus respectively. The threshold of 1 mV m^{-1} is never exceeded in the post noon quadrant for either ECH waves or upper band chorus.

6. Spectral Variation of Wave Amplitudes

[23] Knowledge of the spectral distribution of the wave amplitudes is essential for accurate modeling of the precipitation responsible for the diffuse aurora. Therefore in Figure 5, we present the average equatorial ($-3 < \lambda_m < 3°$) wave amplitudes as a function of normalized frequency and L. The results are shown for, from left to right, the afternoon (1200–1800 MLT), evening (1800–2400), and morning (0000–0600 MLT) sectors for, from top to bottom,

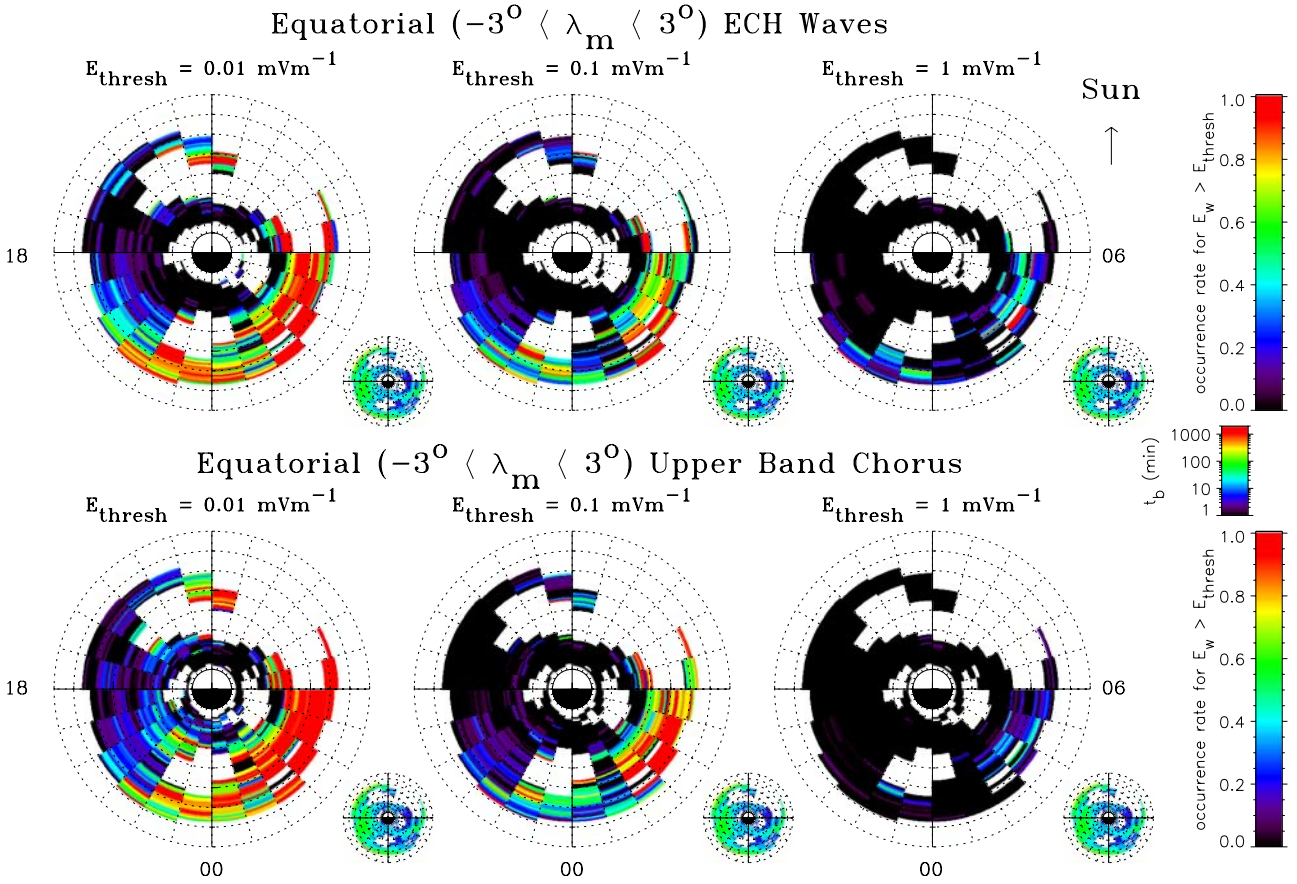

Figure 4. Occurrence rates for equatorial ($-3 < \lambda_m < 3°$) wave amplitudes exceeding a given threshold for (top) ECH waves and (bottom) upper band chorus as a function of L and magnetic local time. The results are shown for active conditions and, from left to right, for threshold amplitudes of 0.01, 0.1, and 1.0 mV m^{-1}. The occurrence rates are shown in the large panels, and the corresponding sampling distributions are in the small panels.

quiet, moderate and active conditions. In each panel the local gyrofrequency and its harmonics are plotted as dashed lines.

[24] The waves are weakest in the afternoon sector (left column) and show little variation with geomagnetic activity. The more intense emissions seen at higher frequencies in this region, particularly during moderate and active conditions, are upper hybrid waves. The waves are more intense in the evening sector (central column) and increase with geomagnetic activity. For each level of activity, there is a tendency for the ECH waves in the first harmonic band to become stronger and peak lower in the band at higher L. In the evening sector the ECH waves are strongest in the first harmonic band during active conditions in the region $6.0 < L < 6.5$, where the wave power is spread over a large fraction of the band. Strong upper band chorus waves are also seen during active conditions, particularly near $L = 5.5$. The upper band chorus power peaks in the range $0.5f_{ce} < f < 0.6f_{ce}$ and decreases with increasing frequency. Overall, the strongest waves tend to be observed in the morning sector (right column). ECH wave emissions in the first harmonic band maximize near the center of the band in the frequency range $1.4f_{ce} < f < 1.8f_{ce}$. ECH emissions are present but weaker in the second harmonic band, while in the higher harmonic bands the emissions maximize low in the band and are associated with periods when the upper hybrid frequency lies in the band. Upper band chorus waves maximize in the frequency band from $0.5f_{ce}$–$0.6f_{ce}$ during active conditions over a range of L, typically from $4.0 < L < 6.0$ and, as in the evening sector, decrease with increasing frequency.

7. Global Morphology of Plasma Sheet Electrons

[25] To determine whether increases in the wave amplitudes are associated with an increase in the resonant electron flux we show the average equatorial, $-15 < \lambda_m < 15°$, perpendicular number flux of (top) 483 eV and (bottom) 5.57 keV electrons in the same format as the wave data in Figure 6. The flux of electrons at both energies shows a pronounced dependence on magnetic local time and L and depends on the level of geomagnetic activity as monitored by AE*. During quiet conditions (left panels) the fluxes are generally low at both energies. Increased fluxes of electrons are seen during moderate conditions in the region $5 < L < 7$ extending from 2100–0700 MLT. The largest fluxes are seen during active conditions (right panels) principally in the early evening to dawn sector for $4 < L < 7$. There is a tendency for the maximum fluxes of lower energy, 483 eV,

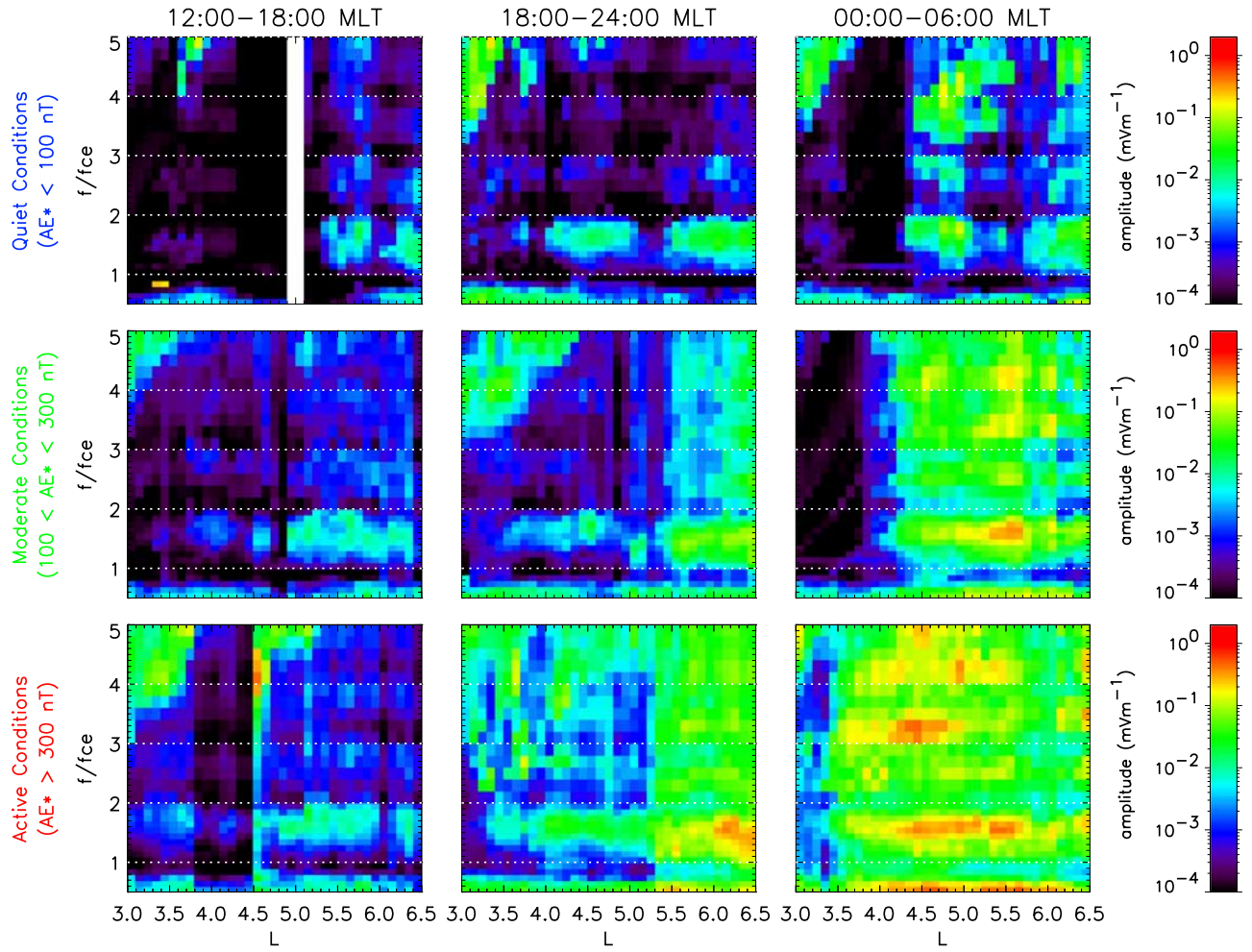

Figure 5. Average equatorial ($-3 < \lambda_m < 3°$) wave amplitudes as a function of frequency and L. The results are shown for, from left to right, the afternoon (1200–1800 MLT), evening (1800–2400), and morning (00–06 MLT) sectors for, from top to bottom, quiet ($AE^* < 100$ nT), moderate ($100 < AE^* < 300$ nT), and active ($AE^* > 300$ nT). In each panel, the local gyrofrequency and its harmonics are plotted as dashed lines.

electrons to penetrate to lower L than the maximum fluxes of the higher energy electrons.

8. Discussion

[26] Excluding the prenoon sector where the wave coverage is poor, we find that the global morphology of the waves and the particles, together with their dependence on geomagnetic activity, is reminiscent of the global morphology of the diffuse aurora as observed from space. For example, the average statistical X ray aurora, corresponding to precipitating electrons with energies in the range $2 < E < 25$ keV, also depends on geomagnetic activity and maximizes during active conditions in the early evening to morning sector over a range of invariant latitudes ($55° < ILAT < 70°$) corresponding to $3 < L < 9$ [*Petrinec et al.*, 1999; *Anderson et al.*, 2001]. Furthermore, the wave intensities and electron fluxes measured by CRRES and the X ray aurora each exhibit a minimum in the dusk quadrant.

[27] During active conditions ECH waves with amplitudes greater than 0.1 mV m^{-1} are present approximately half of the time in the region from 2100–0600 MLT for $4 < L < 7$. Stronger waves, with amplitudes greater than 1 mV m^{-1} are seen in this region for 20% of the observations. Previous studies indicate that these strongest waves are found immediately following substorm injections and subsequently decay on a timescale of several hours [*Meredith et al.*, 2000]. Since scattering rates near the loss cone can approach the strong diffusion limit for ECH waves with amplitudes of the order of 1 mV m^{-1} [*Horne and Thorne*, 2000] the results suggest that ECH waves may result in scattering rates near the strong diffusion limit immediately following substorm injections in the region 2100–0600 MLT with rates falling below the strong diffusion limit at other times when the wave amplitudes are weaker.

[28] Upper band chorus waves with amplitudes greater than 0.1 mV m^{-1} are also seen approximately half of the time during active conditions in the same region as the ECH waves. However, strong upper band chorus waves with amplitudes greater than 1 mV m^{-1} are only seen about 6% of the time. The strongest upper band chorus waves also tend to be observed following substorm injections and subse-

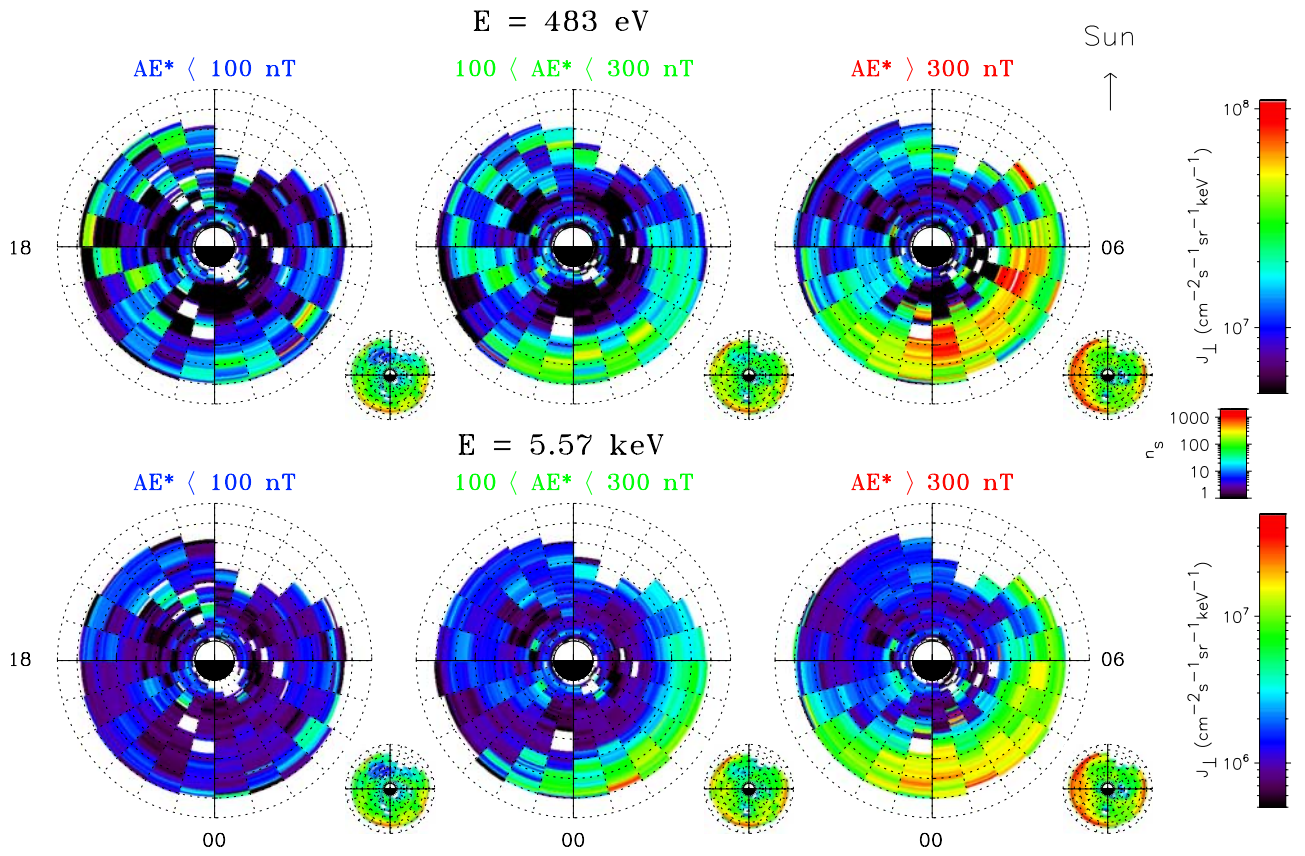

Figure 6. Average equatorial ($-15 < \lambda_m < 15°$) perpendicular differential number flux for (top) 483 eV and (bottom) 5.57 keV electrons as a function of L and magnetic local time. From left to right, the results are presented for quiet ($AE^* < 100$ nT), moderate ($100 < AE^* < 300$ nT), and active ($AE^* > 300$ nT) conditions. The fluxes are shown in the large panels, and the corresponding sampling distributions are in the small panels.

quently decay on a timescale of several hours [*Meredith et al.*, 2000]. Assuming parallel propagation, average upper band chorus amplitudes of 1 mV m^{-1} correspond to magnetic field amplitudes of the order of 30 pT. Since scattering rates near the loss cone exceed the strong diffusion limit for upper band chorus waves with amplitudes of 50 pT [*Ni et al.*, 2008] the results suggest that upper band chorus may result in scattering rates near the strong diffusion limit immediately following substorm injections in the region 2100–0600 MLT, although, as for ECH waves, the rates are likely to fall below the strong diffusion limit at other times when the wave intensities are weaker.

[29] Our results suggest that both ECH waves and upper band chorus will contribute to pitch angle scattering loss approaching the strong diffusion levels [*Horne and Thorne*, 2000; *Ni et al.*, 2008] immediately following substorm injection in the evening to dawn sector but will fall below the strong diffusion level in other regions and at other times. We would therefore expect the precipitating fluxes to maximize during active conditions in this sector, consistent with the location of the peak in the X-ray aurora observed by the PIXIE instrument on the Polar spacecraft [*Petrinec et al.*, 1999; *Anderson et al.*, 2001]. This suggests that energy input into the diffuse aurora should maximize during the declining phase of the solar cycle when high speed solar wind streams from low latitude solar coronal holes drive extended periods of enhanced convection and substorm activity, known as HILDCAA (High Intensity Long Duration Continuous AE Activity) events [e.g., *Tsurutani and Gonzalez*, 1987].

[30] Our statistical analysis, together with the wave spectrogram shown in Figure 1, suggest that ECH waves are present over a wide range of frequencies in the first harmonic band. Frequencies typically maximize in the range $1.4f_{ce} < f < 1.8f_{ce}$, but also extend to higher and lower frequencies. This suggests that ECH waves will scatter electrons at small pitch angles into the loss cone effectively and also scatter electrons over a range of pitch angles from just outside the loss cone up to $\alpha = 60°$ [*Horne and Thorne*, 2000]. For upper band chorus, the pitch angle diffusion coefficients for electrons with energies less than a few keV may exceed the strong diffusion limit over a large range of pitch angles extending from the loss cone to $\alpha = 60° \pm 10°$ [*Ni et al.*, 2008]. These theoretical results suggest that both ECH waves and upper band chorus could lead to the formation of pancake distributions which are observed to form on a timescale of 4 hours following substorm injection in the inner magnetosphere [*Meredith et al.*, 2000].

[31] The statistical distribution of the low energy electrons is consistent with enhanced electron convective injection near midnight followed by subsequent eastward drift around dawn toward the dayside driven by a combination of electric field and magnetic gradient and curvature drifts. During active conditions previously trapped particles may

be lost on a timescale of the order of an hour or so [*Horne and Thorne*, 2000; *Ni et al.*, 2008] leading to scattering loss to the atmosphere on a timescale faster than the drift time to the dayside. Plasma sheet fluxes are subsequently reduced as the particles move from the nightside to the dayside resulting in strong MLT gradients and the formation of pancake distributions as observed.

[32] The ECH waves are strongly confined to the magnetic equatorial plane and peak within ±3° of the magnetic equator. This strong latitudinal confinement is due to the fact that ECH waves propagate almost perpendicular to the ambient magnetic field and wave growth is tightly confined to within a few degrees of the magnetic equator [*Horne*, 1988, 1989, 1990; *Horne et al.*, 2003]. Indeed, the location of the peak ECH wave power may provide a more accurate measurement of the true location of the magnetic equator than provided by magnetic field models [e.g., *Gough et al.*, 1979; *Christiansen et al.*, 1978; *Paranicas et al.*, 1992; *Meredith et al.*, 2000]. The upper band chorus waves are also confined to the magnetic equatorial plane, though less strongly than the ECH waves, and tend to peak within ±5° of the magnetic equator. The latitudinal distribution of chorus is controlled by Landau damping by suprathermal electrons [*Bortnik et al.*, 2007]. This process is most severe on the nightside at high frequency, which strongly confines upper band chorus to locations near the magnetic equator.

[33] The lower panels of Figure 2 show that there is a rather sharp cutoff in the average wave amplitudes of upper band chorus at x ~2.6, corresponding to a gyrofrequency cutoff of ~50 kHz. Waves in the band $0.5f_{ce} < f < f_{ce}$ fall in the range 25–50 kHz at this location. At higher values of x the frequency band of upper band chorus falls to lower frequencies and starts to include VLF transmitter signals which are typically observed in the frequency range 10 kHz < f < 25 kHz. It is interesting to note that the additional weak wave power extending to higher latitudes in the region $2.6 < x < 3.0$ has a similar distribution to CRRES observations of the nonducted wave power from the NAA transmitter in Maine USA (not shown) which operates at 24.0 kHz [*Clilverd et al.*, 2008].

[34] Our study suggests that both ECH waves and whistler mode chorus are likely to play important roles in the production of the diffuse aurora. Diffusion rates may exceed the strong diffusion limits during active conditions (AE^* > 300 nT) which are associated with injection events, but are likely to remain below the strong diffusion level at other times. More detailed modeling work using measured wave spectral properties as a function of spatial location and geomagnetic activity are required to accurately quantify the rates of pitch angle scattering by ECH waves and upper band chorus and to determine their respective roles in the production of the diffuse aurora.

9. Conclusions

[35] We have examined wave and particle data from the CRRES spacecraft to estimate the likely roles of ECH waves and upper band chorus in the production of the diffuse aurora. Our main conclusions are:

[36] 1. Both ECH waves and upper band chorus increase with increasing geomagnetic activity suggesting they are related to periods of enhanced convection and/or substorm activity. Intensities maximize during active conditions (AE^* > 300 nT) with peak amplitudes of the order of 1 mV m^{-1}.

[37] 2. The waves are confined to the equatorial region with ECH waves being typically confined to ±3° of the magnetic equator and upper band chorus being confined to ±5° of the magnetic equator.

[38] 3. The narrow equatorial confinement of the waves excludes the prenoon sector (0600 to 1200 MLT) from the analysis. Noting this limitation, we find that the wave amplitudes peak outside L = 4 during active conditions from 2100 to 0600 MLT for both upper band chorus and ECH waves.

[39] 4. During active conditions in the region $4 < L < 7$ from 2100 to 0600 MLT the equatorial wave amplitudes exceed 0.1 mV m^{-1} approximately 50% of the time for both wave modes. However, the strongest wave amplitudes, exceeding 1 mV m^{-1}, are more common for ECH waves (20% of the time) than for upper band chorus (6% of the time).

[40] 5. Upper band chorus waves are typically observed from $0.5f_{ce}$ to f_{ce} but the amplitudes maximize between $0.5f_{ce}$ and $0.6f_{ce}$ and decrease with increasing frequency. ECH waves in the first harmonic band are observed from just above f_{ce} to just below f_{ce}. They typically peak between $1.4f_{ce}$ and $1.8f_{ce}$.

[41] 6. Excluding the prenoon sector due to lack of wave coverage, we find that enhanced fluxes of plasma sheet electrons (100 eV < E < 30 keV) are observed during active conditions in the same region of geospace as the enhanced waves.

[42] 7. The patterns of the upper band chorus, ECH waves and plasma sheet electrons are similar to the global morphology of the diffuse aurora.

[43] Both ECH waves and upper band chorus contribute to the diffuse aurora. Diffusion rates may exceed the strong diffusion limits during injection events but are likely to remain below the strong diffusion level at other times. To determine the precise role of these waves in the production of the diffuse aurora measured wave spectral profiles should be used in diffusion codes to estimate the rates of pitch angle scattering as a function of spatial location, magnetic activity, energy and pitch angle.

[44] **Acknowledgments.** We thank the NSSDC Omniweb for providing the *AE* indices used in this paper. This work was supported by the Natural Environment Research Council and NSF grant ATM 0802843.

[45] Wolfgang Baumjohann thanks Ondrej Santolik and Larry Lyons for their assistance in evaluating this paper.

References

Anderson, R. R., and K. Maeda (1977), VLF emissions associated with enhanced magnetospheric electrons, *J. Geophys. Res.*, *82*, 135–146.

Anderson, R. R., D. A. Gurnett, and D. L. Odem (1992), CRRES plasma wave experiment, *J. Spacecr. Rockets*, *29*, 570–573.

Anderson, P. C., S. M. Petrinec, and K. Liou (2001), Statistical patterns in X ray and auroral emissions and energetic particle precipitation, *J. Geophys. Res.*, *106*, 5907–5911.

Ashour-Abdalla, M., and C. F. Kennel (1978), Nonconvective and convective electron cyclotron harmonic instabilities, *J. Geophys. Res.*, *83*, 1531–1543.

Belmont, G., D. Fontaine, and P. Canu (1983), Are electron cyclotron waves responsible for diffuse auroral electron precipitation?, *J. Geophys. Res.*, *88*, 9163–9169.

Belmont, G., D. Fontaine, and P. Canu (1984), Reply to comment on "Are electron cyclotron waves responsible for diffuse auroral electron precipitation?", *J. Geophys. Res.*, *89*, 7591–7592.

Bortnik, J., R. M. Thorne, and N. P. Meredith (2007), Modeling the propagation characteristics of chorus using CRRES suprathermal electron fluxes, *J. Geophys. Res.*, *112*, A08204, doi:10.1029/2006JA012237.

Chen, M. W., and M. Schulz (2001a), Simulations of storm time diffuse aurora with plasma sheet electrons in strong pitch angle diffusion, *J. Geophys. Res.*, *106*, 1873–1886.

Chen, M. W., and M. Schulz (2001b), Simulations of diffuse aurora with plasma sheet electrons in pitch angle diffusion less than everywhere strong, *J. Geophys. Res.*, *106*, 28,949–28,966.

Christiansen, P. J., M. P. Gough, G. Martelli, J. J. Bloch, N. Cornilleau, J. Etcheto, R. Gendrin, C. Beghin, P. Decreau, and D. Jones (1978), GEOS-1 Observations of electrostatic waves, and their relationship with plasma parameters, *Space Sci. Rev.*, *22*, 383–400.

Clilverd, M. A., C. J. Rodger, R. Gamble, N. P. Meredith, M. Parrot, J.-J. Berthelier, and N. R. Thomson (2008), Ground-based transmitter signals observed from space: Ducted or nonducted, *J. Geophys. Res.*, *113*, A04211, doi:10.1029/2007JA012602.

Fontaine, D., and M. Blanc (1983), A theoretical approach to the morphology and dynamics of diffuse auroral zones, *J. Geophys. Res.*, *88*, 7171–7184.

Frahm, R. A., J. D. Winninghham, J. R. Sharber, R. Link, G. Crowley, E. E. Gaines, D. L. Chenette, B. J. Anderson, and T. A. Poterma (1997), The diffuse aurora: A significant source of ionisation in the middle atmosphere, *J. Geophys. Res.*, *102*, 28,203–28,214.

Fredricks, R. W., and F. L. Scarf (1973), Recent studies of magnetospheric electric field emissions above the electron gyrofrequency, *J. Geophys. Res.*, *78*, 310–314.

Gough, M. P., P. J. Christiansen, G. Martelli, and E. J. Gershuny (1979), Interaction of electrostatic waves with warm electrons at the geomagnetic equator, *Nature*, *279*, 515–517.

Gurnett, D. A., and R. R. Shaw (1973), Electromagnetic radiation trapped in the magnetosphere above the plasma frequency, *J. Geophys. Res.*, *78*(34), 8136–8149.

Gurnett, D. A., R. R. Anderson, B. T. Tsurutani, E. J. Smith, G. Paschmann, G. Haerendel, S. J. Bame, and C. T. Russell (1979), Plasma wave turbulence at the magnetopause: Observations from ISEE 1 and 2, *J. Geophys. Res.*, *84*, 7043–7058.

Hardy, D. A., D. M. Walton, A. D. Johnstone, M. F. Smith, M. P. Gough, A. Huber, J. Pantazis, and R. Burkhardt (1993), The low energy plasma analyser, *IEEE Trans. Nucl. Sci.*, *40*(2), 246–251.

Horne, R. B. (1988), Ray tracing of electrostatic waves in a hot plasma and its application to the generation of terrestrial myriametric radiation, *Geophys. Res. Lett.*, *15*, 553–556.

Horne, R. B. (1989), Path-integrated growth of electrostatic waves: The generation of terrestrial myriametric radiation, *J. Geophys. Res.*, *94*, 8895–8909.

Horne, R. B. (1990), Narrow-band structure and amplitude of terrestrial myriametric radiation, *J. Geophys. Res.*, *95*, 3925–3932.

Horne, R. B., and R. M. Thorne (2000), Electron pitch angle diffusion by electrostatic electron harmonic waves: The origin of pancake distributions, *J. Geophys. Res.*, *105*, 5391–5402.

Horne, R. B., P. J. Christiansen, M. P. Gough, K. Rönnmark, J. F. E. Johnson, J. Sojka, and G. L. Wrenn (1981), Amplitude variations of electron cyclotron harmonic waves, *Nature*, *294*, 338–340.

Horne, R. B., R. M. Thorne, N. P. Meredith, and R. R. Anderson (2003), Diffuse auroral electron scattering by electron cyclotron harmonic and whistler mode waves during an isolated substorm, *J. Geophys. Res.*, *108*(A7), 1290, doi:10.1029/2002JA009736.

Hubbard, R. F., and T. J. Birmingham (1978), Electrostatic emissions between electron gyroharmonics in the outer magnetosphere, *J. Geophys. Res.*, *83*, 4837–4850.

Inan, U., Y. Chiu, and G. Davidson (1992), Whistler-mode chorus and morning-side aurorae, *Geophys. Res. Lett.*, *19*, 653–656.

Johnson, M. H., and J. Kierein (1992), Combined Release and Radiation Effects Satellite (CRRES), Spacecraft and mission, *J. Spacecr. Rockets*, *29*, 556–563.

Johnstone, A. D., D. M. Walton, R. Liu, and D. Hardy (1993), Pitch angle diffusion of low-energy electrons by whistler mode waves, *J. Geophys. Res.*, *98*, 5959–5967.

Kennel, C. F., F. L. Scarf, R. W. Fredricks, J. H. Mcghee, and F. V. Coroniti (1970), VLF electric field observations in the inner magnetosphere, *J. Geophys. Res.*, *75*, 6136–6152.

Koons, H. C., and J. L. Roeder (1990), A survey of equatorial magnetospheric wave activity between 5 and 8 R_E, *Planet. Space Sci.*, *38*, 1335–1341.

Lam, M. M., R. B. Horne, N. P. Meredith, and S. A. Glauert (2007), Modeling the effects of radial diffusion and plasmaspheric hiss on outer radiation belt electrons, *Geophys. Res. Lett.*, *34*, L20112, doi:10.1029/2007GL031598.

Lyons, L. R. (1974), Electron diffusion driven by magnetospheric electrostatic waves, *J. Geophys. Res.*, *79*, 575–580.

Lyons, L. R. (1984), Comment on "Are equatorial electron cyclotron waves responsible for diffuse precipitation?", *J. Geophys. Res.*, *89*, 7589.

Lyons, L. R., and R. M. Thorne (1973), Equilibrium structure of radiation belt electrons, *J. Geophys. Res.*, *78*, 2142–2149.

Meredith, N. P., A. D. Johnstone, S. Szita, R. B. Horne, and R. R. Anderson (1999), "Pancake" electron distributions in the outer radiation belts, *J. Geophys. Res.*, *104*, 12,431–12,444.

Meredith, N. P., R. B. Horne, A. D. Johnstone, and R. R. Anderson (2000), The temporal evolution of electron distributions and associated wave activity following substorm injections in the inner magnetosphere, *J. Geophys. Res.*, *105*, 12,907–12,917.

Meredith, N. P., R. B. Horne, and R. R. Anderson (2001), Substorm dependence of chorus amplitudes: Implications for the acceleration of electrons to relativistic energies, *J. Geophys. Res.*, *106*, 13,165–13,178.

Meredith, N. P., R. B. Horne, S. A. Glauert, R. M. Thorne, D. Summers, J. M. Albert, and R. R. Anderson (2006), Energetic outer zone electron loss timescales during low geomagnetic activity, *J. Geophys. Res.*, *111*, A05212, doi:10.1029/2005JA011516.

Meredith, N. P., R. B. Horne, S. A. Glauert, and R. R. Anderson (2007), Slot region electron loss timescales due to plasmaspheric hiss and lightning generated whistlers, *J. Geophys. Res.*, *112*, A08214, doi:10.1029/2006JA012413.

Meredith, N. P., R. B. Horne, S. A. Glauert, D. N. Baker, S. G. Kanekal, and J. M. Albert (2009), Relativistic electron loss timescales in the slot region, *J. Geophys. Res.*, *114*, A03222, doi:10.1029/2008JA013889.

Ni, B., R. M. Thorne, Y. Y. Shprits, and J. Bortnik (2008), Resonant scattering of plasma sheet electrons by whistler-mode chorus: Contribution to diffuse auroral precipitation, *Geophys. Res. Lett.*, *35*, L11106, doi:10.1029/2008GL034032.

Olson, W. P., and K. Pfitzer (1977), Magnetospheric magnetic field modeling, Annual Scientific Report, AFOSR Contract Number F44620-75-c-0033.

Paranicas, C., W. J. Hughes, H. J. Singer, and R. R. Anderson (1992), Banded electrostatic emissions observed by the CRRES plasma wave experiment, *J. Geophys. Res.*, *97*, 13,889–13,898.

Peticolas, L. M., T. J. Hallinan, H. C. Stenbaek-Nielsen, J. W. Bonnell, and C. W. Carson (2002), A study of black aurora from aircraft-based optical observations and plasma measurements on FAST, *J. Geophys. Res.*, *107*(A8), 1217, doi:10.1029/2001JA900157.

Petrinec, S. M., D. L. Chenette, J. Mobilia, M. A. Rinaldi, and W. L. Imhof (1999), Statistical X ray auroral emissions — PIXIE observations, *Geophys. Res. Lett.*, *26*, 1565–1568.

Roeder, J. L., and H. C. Koons (1989), A survey of electron cyclotron waves in the magnetosphere and the diffuse auroral precipitation, *J. Geophys. Res.*, *94*, 2529–2541.

Rönnmark, K., and P. J. Christiansen (1981), Dayside electron cyclotron harmonic emissions, *Nature*, *294*, 335–338.

Sandford, B. P. (1968), Variations of auroral emissions with time, magnetic activity and the solar cycle, *J. Atmos. Sol.-Terr. Phys.*, *30*, 1921–1942.

Sergienko, T., I. Sandahl, B. Gustavsson, L. Andersson, U. Brandstrom, and A. Steen (2008), A study of fine structure of diffuse aurora with ALIS-FAST measurements, *Ann. Geophys.*, *26*, 3185–3195.

Shaw, R. R., and D. Gurnett (1975), Electrostatic noise bands associated with the electron gyrofrequency and plasma frequency in the outer magnetosphere, *J. Geophys. Res.*, *80*, 4259–4271.

Summers, D., B. Ni, and N. P. Meredith (2007), Timescales for radiation belt electron acceleration and loss due to resonant wave-particle interactions: 2. Evaluation for VLF chorus, ELF hiss, and electromagnetic ion cyclotron waves, *J. Geophys. Res.*, *112*, A04207, doi:10.1029/2006JA011993.

Tsurutani, B. T., and E. J. Smith (1974), Postmidnight chorus: A substorm phenomenon, *J. Geophys. Res.*, *79*, 118–127.

Tsurutani, B. T., and E. J. Smith (1977), Two types of magnetospheric ELF chorus and their substorm dependencies, *J. Geophys. Res.*, *82*, 5112–5128.

Tsurutani, B. T., and W. D. Gonzalez (1987), The cause of high intensity long duration continuous AE activity (HILDCAAs): Interplanetary Alfven wave trains, *Planet. Space Sci.*, *35*, 405–412.

Wrenn, G. L., J. F. E. Johnson, and J. J. Sojka (1979), Stable "pancake" distributions of low energy electrons in the plasma trough, *Nature*, *279*, 512.

R. R. Anderson, Department of Physics and Astronomy, University of Iowa, 615 Van Allen Hall, Iowa City, IA 52242-1479, USA. (roger-r-anderson@uiowa.edu)

R. B. Horne and N. P. Meredith, British Antarctic Survey, Natural Environment Research Council, Madingley Road, Cambridge CB3 0ET, UK. (r.horne@bas.ac.uk; nmer@bas.ac.uk)

R. M. Thorne, Department of Atmospheric and Oceanic Sciences, University of California, Los Angeles, 405 Hilgard Avenue, Los Angeles, CA 90095-1565, USA. (rmt@atmos.ucla.edu)